Journal of ELECTRONIC MATERIALS, Vol. 46, No. 8, 2017
DOI: 10.1007/s11664-017-5491-z

One-Dimensional Metal-Oxide Nanostructures for Solar Photocatalytic Water-Splitting

FENGYUN WANG,[1,3] LONGFEI SONG,[1] HONGCHAO ZHANG,[1] LINQU LUO,[1] DONG WANG,[1] and JIE TANG[2]

1.—College of Physics and Cultivation Base for State Key Laboratory, Qingdao University, Qingdao 266071, China. 2.—National Institute for Materials Science (NIMS), Sengen 1-2-1, Tsukuba, Ibaraki 305-0047, Japan. 3.—e-mail: fywang@qdu.edu.cn

Because of their unique physical and chemical properties, one-dimensional (1-D) metal-oxide nanostructures have been extensively applied in the areas of gas sensors, electrochromic devices, nanogenerators, and so on. Solar water-splitting has attracted extensive research interest because hydrogen generated from solar-driven water splitting is a clean, sustainable, and abundant energy source that not only solves the energy crisis, but also protects the environment. In this comprehensive review, the main synthesis methods, properties, and especially prominent applications in solar water splitting of 1-D metal-oxides, including titanium dioxide (TiO_2), zinc oxide (ZnO), tungsten trioxide (WO_3), iron oxide (Fe_2O_3), and copper oxide (CuO) are fully discussed.

Key words: One-dimensional, metal-oxide, nanostructures, solar water-splitting

INTRODUCTION

As the global population increases, energy demands are also continuously increasing. Renewable solar energy is believed to be a potential solution to energy sustainability and environment protection. Solar-to-chemical energy conversion is considered the same goal for researchers who focus on energy generation.[1] Sunlight is the ideal limitless and carbon-neutral energy source with sufficient scale to replace fossil fuels and satisfy increasing global energy demands.[2–4] In recent years, artificial photosynthesis (APS) has become a potentially controllable approach for solar-to-chemical energy conversion which emulates the natural photosynthesis process using man-made materials.

Photoelectrochemical (PEC) water splitting produces hydrogen through solar energy. It is a typical process of artificial photosynthesis in which solar energy is converted into chemical fuels. The oxidation of water to O_2 is an important process in the direct PEC production of fuels from sunlight.[5,6] Water cannot be directly decomposed by light with wavelength shorter than 190 nm. However, for electrochemical water electrolysis in the presence of photocatalyst, only a minimum voltage, equivalent to the energy irradiance with a wavelength of ~1000 nm, is needed.[7] Hence, water-splitting can be achieved using visible light irradiation with the participation of a suitable photocatalyst. The artificial photosynthesis that generated H_2 was firstly reported in 1971 by Honda and Fujishima, who used TiO_2 film as a photoanode and no other co-catalysts on the TiO_2 surface in a PEC cell.[8] As shown in the Fig. 1, water is oxidized on the anodic titania, $2H^+ + H_2O \rightarrow 1/2O_2 + 2H^+$, and the protons are reduced at the other electrode to produce hydrogen, $2e^- + 2H^+ \rightarrow H_2$.

As the development of 1-D metal oxides has matured, superior performances in water splitting has been widely reported.[9–11] Metal oxides are typical ionic compounds comprising positive metallic and negative oxygen ions, in which the positive metallic ions and the negative oxygen ions interact with each other. Most of the metal oxides have fantastic thermal and chemical stability, and

(Received August 27, 2016; accepted March 28, 2017; published online April 10, 2017)

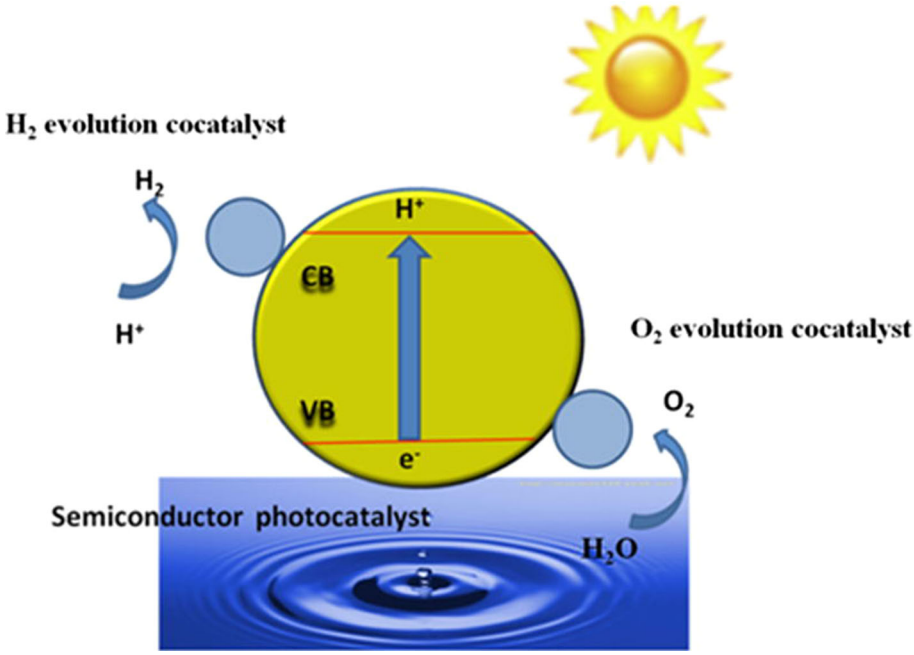

Fig. 1. Schematic diagram of solar-driven water splitting using a semiconductor photocatalyst.

variety of excellent properties including wide band-gaps, high dielectric constants, high carrier concentration, good electrical, optical, and electrochromic characteristics on account of its completely filled s-shells.[12–14] Hence, 1-D metal oxides are regarded as one of the most excellent functional materials and have been extensively exploited in multifarious technological applications.[15] Significant progress in the fabrication of 1-D mental oxides have provided simple and efficient hetero-nanostructures for solar water-spitting with photocurrents ranging from microamperes to milliamperes per square centimeter.[16–18]

Here, we systematically introduce some recent developments of properties, synthesis methods, and primarily applications in water splitting of some typical 1-D metal oxides, including TiO_2, ZnO, WO_3, $Fe_{1-x}O$, and CuO.

TIO_2

Titanium oxides have different chemical forms which can be categorized into typical TiO_2[19–21] and Ti_nO_{2n-1}[22] forms, such as TiO,[22] Ti_2O_3,[23] Ti_3O_5,[24] Ti_4O_7,[25] Ti_5O_9,[26] Ti_7O_{13},[27] and Ti_9O_{17}.[28] Titanium oxides also exist in various crystalline phases, such as tetragonal, orthorhombic, monoclinic, hexagonal, triclinic, and rhombohedra. However, TiO_2 is composed of octahedrals with shared oxygen atoms and is mainly sorted into three crystalline structures of rutile (tetragonal structure), anatase (tetragonal structure), and brookite (orthorhombic structure), respectively. TiO_2 is composed of octahedrals with shared oxygen atoms. The neighboring rutile octahedrals share corners along the [110] directions, while the anatase shares corners along the (110) planes. TiO_2, especially 1-D TiO_2 due to the quantum confined effect, performs outstandingly in photovoltaic,[29] photocatalytic,[30] gas sensing,[31,32] and electrochromic devices.[32,33]

Recently, enormous efforts have been made to synthesize 1-D TiO_2 in the form of nanorods, NWs, nanofibers, nanobelts, and nanotubes. TiO_2 has been extensively studied in photocatalytic and photoeletrochemical production of hydrogen due to its chemical stability, high efficiency, and low cost.[34–37] Since the practical demonstration of PEC water splitting was reported by Honda and Fujishima,[38] extensive research efforts have been concentrated on preparation and development of the nanostructure of 1-D TiO_2 materials for efficient light harvesting, high quantum efficiency, practical stability, low-cost fabrication, and especially, enhanced PEC water splitting performances.[39] 1-D TiO_2 nanowires have showed high water splitting photoactivity due to their plentiful oxide vacancies currently. A photocurrent of approximately 1.3 mA cm^{-2} at 0.7 V·vs was obtained from a reversible hydrogen electrode (RHE) measured in 1 M KOH under simulated AM 1.5G full spectrum irradiation (light intensity of 100 mW cm^{-2}), which corresponds to an applied bias-compensated photon-to-current efficiency (ABPCE) of approximately 0.69%.

An et al. used 1-D TiO_2 NWs with high electron mobility to construct $TiO_2/BiVO_4$ heterostructures with designed interfacial defects that efficiently increased the carrier concentration and extend the

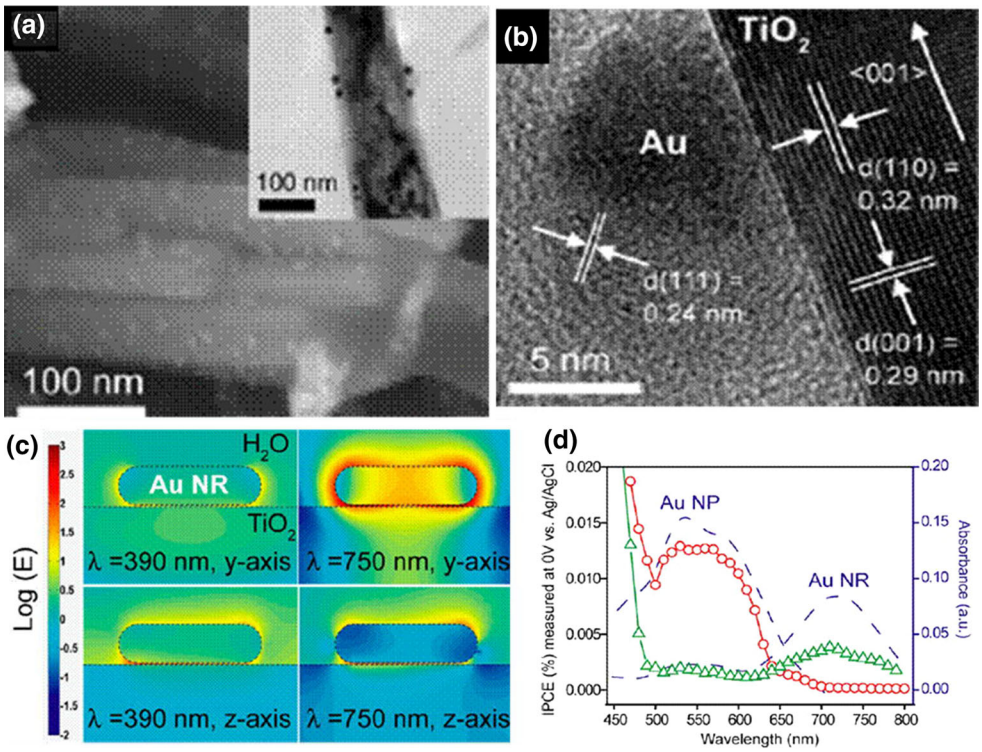

Fig. 2. (a) SEM and TEM (inset) images of Au NP-decorated TiO_2 NWs. (b) HRTEM image taken at the interface between Au NP and TiO_2 NW. (c) Spatial distribution of electric field on the y–z plane for NP-TiO_2 and NR-TiO_2 NWs. The incident light is along a specific direction (y or z axis). (d) Magnified IPCE plots of NP-2-TiO_2 and NR-TiO_2 electrodes in the incident wavelength between 450 nm and 800 nm, highlighted by the dashed box in panel a. The corresponding absorption spectra of NP-2-TiO_2 and NR-TiO_2 are also included for comparison. Reprinted from Ref. 40. Copyright 2013 American Chemical Society.

lifetime of electrons. The inherent phenomenon of defective electronic structures in different heterostructures creates a significant change in their photoelectrochemical performance and produces a high photocurrent of 2.24 mA cm^{-2}. The $TiO_2/BiVO_4$ heterostructure has significantly higher photoconversion efficiency than bare TiO_2 NWs. Ying-Chih Pu et al. reported that the photoactivity of Au nanoparticle (NPs)-decorated TiO_2 electrodes for photoelectrochemical water splitting can be obviously enhanced in the whole UV–visible region by adjust and control the shape of the decorated Au nanoparticles prepared. This is accomplished by immersing NWs into a $HAuCl_4$ solution to form $AuCl(OH)_{3^-}$ complex on the TiO_2 surface, followed by annealing at 300°C.[34,40] The prepared Au NPs which were deposited on the surface of TiO_2 NWs possessed a typical size of ~8 nm. In the Fig. 2b, the high-resolution transmission electron microscopy (HRTEM) image taken at the interface of NW and NP regions clearly reveals that high quality rutile TiO_2 and face-centered cubic Au crystals can be obtained by this facile technique. Figure 2c shows the spatial distribution of electric-field intensity at the Au/TiO_2 interface as monochromatic incident light travels along a fixed direction. The electric field intensity at the interface was increased by 15 times the magnitude under incident light of 750 nm. This is important for both Au NP- and Au nanorods (NR-) decorated TiO_2 NWs, and could explain the mechanism of enhanced visible light photoactivity, in spite of no spectral overlap between the amplified electric field and the absorption edge of TiO_2. Nevertheless, it is well-known that there are defect states within the band gap of TiO_2.[41,42] Figure 2d displays that Au NP- and Au NR-decorated TiO_2 electrodes possess incident photon-to-current efficiency (IPCE) peaks at various incident light wavelengths, which can match well with the corresponding surface plasmon resonance (SPR) absorption peaks in the visible region. These results indicate that the photoactivity of Au-decorated TiO_2 NW electrodes for PEC water splitting can be effectively improved in the whole UV–visible region by decorating with various shapes of Au nanostructures. Au acts as an antenna that localizes the optical energy by surface plasmon resonance (SPR). Plasmonic Au can sensitize TiO_2 to light with energy below the band gap, generating charge for water splitting. This may effectively solve the disadvantage of the wide band gap of TiO_2, even though it is expensive to add Au nanostructures. Thus, it has potential to prepare composite plasmonic metal photoelectrodes to use solar energy effectively.

ZNO

Zinc oxides contains two chemical forms, ZnO and ZnO_2, with only two crystalline phases, hexagonal and cubic crystals. Zinc oxides are also widely used in the photocatalytic and PEC arenas.[43–47] 1-D zinc oxides can be formed into nanorods,[48,49] NWs,[50] nanonails,[51] nanopencils,[51] nanobullets,[52] nanotubes,[53] nanocomb-bike structures,[54,55] nanoribbons,[56] nanobelts,[57] nanopins,[58] nanoneedles,[59] etc., by two principal methods: condensation processes (top-down strategy) and the solution-phase method (bottom-up strategy).[60] Because of the near-UV emission, optical transparency, electric conductivity, and high stability, 1-D zinc oxide (ZnO) nanostructures have been considered one of the most potentially multifunctional materials[61] with huge applicable potential in sensors,[62] optoelectronics,[63] field emission,[64] solar cells,[65] and surface acoustic waveguides.[66–68] Xu et al.[60] applied wet-chemical treatment methods to in situ decorate $ZnFe_2O_4$ film onto conductive 5% Al-doped ZnO NW (Al:Zn) arrays for solar-driven water splitting. The Al:ZnO nanowires were fabricated by using the hydrothermal method. Because of the high conductivity of Al:ZnO and visible-spectrum absorption of the $ZnFe_2O_4$ film, this unique structure shows excellent properties with low onset potential (V_{RHE} = 0.38 V) and high photocurrent densities of 1.72 mA cm^{-2} (V_{RHE} = 1.23 V) (Fig. 3a). The applied bias photon-to-current efficiency (ABPE) plots of various photoanodes are shown in Fig. 3b. The maximum applied bias photon-to-current efficiency (ABPE) can reach up to 0.28% when using a photoanode of AZO-ZFO-3 min (5% Al:ZnO-$ZnFe_2O_4$) at the external bias of 0.86 V, which is enhanced ~600% above the pristine 5% Al-doped ZnO nanowires (AZO) film (0.047%). This work predicts that the photocatalytic performance of photoanodes can be enhanced by doping and decorating the surfaces of ZnO NWs. Coincidentally, this year, Lee et al.[69] employed ferroelectric phase transformed Li-doped ZnO NWs as photoanodes for PEC water splitting and systematically investigated their poling effects. Solar-to-hydrogen efficiencies from water splitting were improved by 200% compared with a negatively poled electrode.

WO_3

Tungsten oxides is very interesting and have been extensively investigated among transition metal oxides because of their unique physical and chemical properties. Tungsten oxides have various chemical forms, including WO_2,[70] WO_3,[71] W_2O_5,[72] $W_{18}O_{49}$,[73] W_3O_8,[74] W_5O_{14},[75] and $WO_{2.9}$,[76] in different crystalline phases including monoclinic, triclinic, orthorhombic, and tetragonal crystals during various transition temperatures.[77] Nanostructured tungsten oxides are known by their unique chemical and physical properties. 1-D WO_3

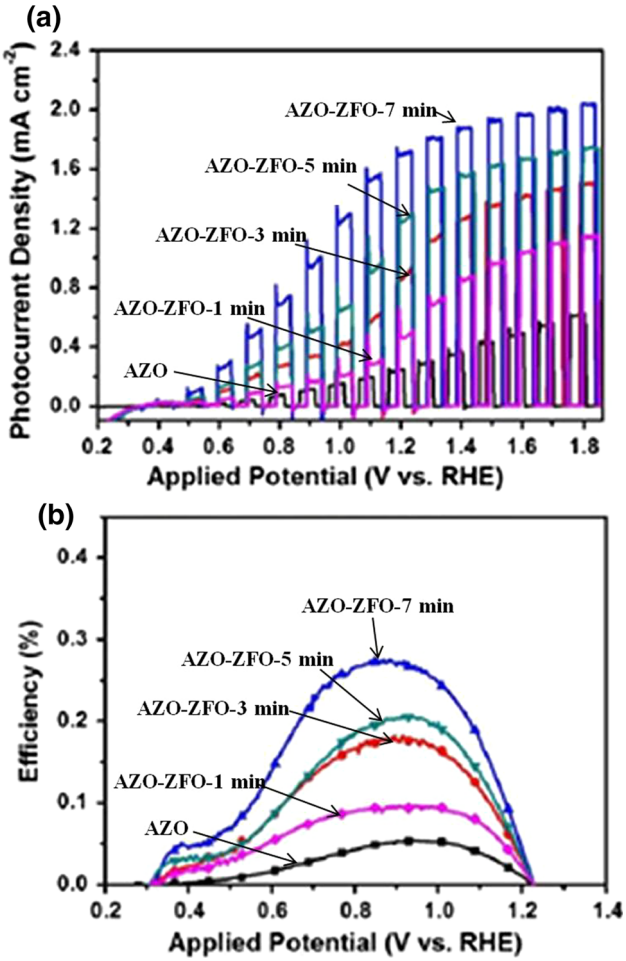

Fig. 3. (a) Linear sweep voltammetry (LSV) plots of 0.5% Al-doped ZnO nanowires (AZO) and Al-doped ZnO-$ZnFe_2O_4$ (AZO-ZFO) photoanodes under chopped illumination. The treating time of AZO-ZFO is 1 min, 3 min, 5 min, 7 min, respectively. The concentration of Al element increases while the treating time increases. (b) The corresponding applied bias photo-to-current (ABPE) plots. Reprinted from Ref. 60. Copyright 2016 Royal Society of Chemistry.

nanostructures show greatly potential as photocatalysts, especially in water splitting. The synthesis of 1-D nanostructures, assembled into ordered superstructures or complex functional architectures, give us opportunities to explore their unique properties and to fabricate nanodevices. Various synthesis methods, such as thermal treatment, vapor phase growth, solvothermal synthesis with raw materials, chemical vapor deposition (CVD) process, have been developed to prepare nanotubes, nanobelts, nanorods, NWs, nanotips, etc.[78–82] For example, Fig. 4 is a schematic of the hot filament CVD (HFCVD) technique applied to synthesize WO_3 NWs on Si wafers. Hot-filament CVD can be considered as one of the CVD techniques due to its similarity. However, the hot-filament in HFCVD is not only as hot energy source but also as metal-vapor source during deposition.

In recent years, reports on WO_3 with applications to water splitting have been numerous.[78,79,81,83] Rao

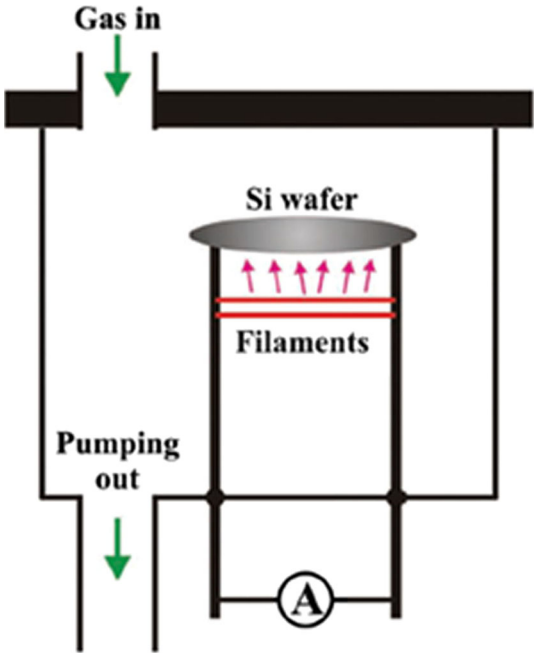

Fig. 4. Hot filament CVD technique. Reprinted from Ref. 77. Copyright 2012 John Wiley and Sons.

et al.[83] tested a photoanode with the highest reported product ($\eta_{abs} \times \eta_{sep}$ = 53%) of $BiVO_4$-based photoanodes, by coating a thin layer of $BiVO_4$ onto a vertical array of electrically conductive WO_3 NWs to prepare WO_3/W-doped $BiVO_4$ core/shell structured NWs (WO_3/W:$BiVO_4$ NWs, Fig. 5a). $BiVO_4$ is the primary light absorber and WO_3 NWs act as an electron conductor. As we can see in Fig. 5a, core/shell NWs are built with multiple changes for improving charge separation in $BiVO_4$, including thickness reduction, nanoscale porosity addition, heterojunction formation, and gradient doping on prepared structure. The light absorption efficiency of the present WO_3/W:$BiVO_4$ NWs photoanodes is relatively high due to the superior morphology which optimizes light absorption and carriers transport at the same time. The WO_3/W:$BiVO_4$ NWs were prepared by a combination of flame vapor deposition and drop-casting approaches. The flame-synthesis method is essential for practical applications due to its high efficiency, low-cost and accuracy. The as-grown $W_{18}O_{49}$ NWs were further annealed in air at 550°C in a box furnace for 2 h, and stoichiometric and crystalline WO_3 NWs were are obtained after that (Fig. 5b). As shown in Fig. 5c, after all the coating steps, the prepared samples were annealed in air at 550°C for 2 h to obtain a crystalline W-doped $BiVO_4$ shell composed by a single layer of densely packed nanoparticles on WO_3 NWs. Figure 5d shows that the photocurrent of the final fabricated WO_3/W:$BiVO_4$ core/shell NWs reaches 3.1 mA cm^{-2} at a potential of 1.23 V versus RHE under the simulated AM 1.5G illumination. In this study, the critical advancement is an application of

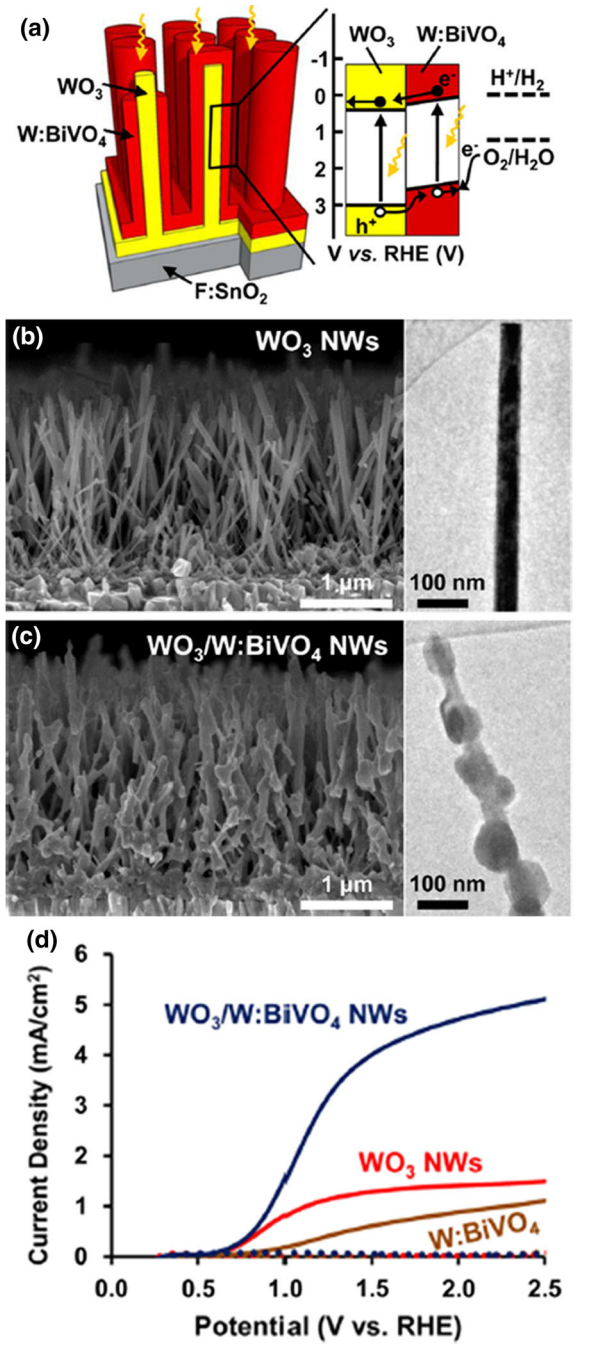

Fig. 5. The WO_3/W:$BiVO_4$ core/shell NWs photoanode. (a) Structural schematic and energy band structure of the core/shell NWs and type-II staggered heterojunction, in which charges generated in both the W:$BiVO_4$ shells and WO_3 NW cores can contribute to the water oxidation photocurrent. The band edges and water oxidation or reduction potentials are plotted on the reversible hydrogen electrode (RHE) scale. (b, c) Scanning electron microscope (SEM, left) and transmission electron microscope (TEM, right) images of the bare WO_3 NW array (75 nm average NW diameter) and WO_3/W:$BiVO_4$ core/shell NWs (60 nm average W:$BiVO_4$ shell thickness), respectively. The W:$BiVO_4$ shell consists of a single layer of densely packed nanoparticles. (d) Photoelectrochemical response of the WO_3/W:$BiVO_4$ NW photoanode and control the sample in 0.5 M potassium phosphate electrolyte buffered to pH 8. Current–voltage (J–V) curves (solid lines: simulated AM 1.5G illumination, dotted lines: dark). Reprinted from Ref. 83. Copyright 2014 American Chemical Society.

electrically conductive WO_3 NW array to offset the intrinsically poor properties of charge transport in $BiVO_4$ without compromising light absorption. Therefore, the result they obtained can achieve η_{abs} of 69% and η_{sep} of 77% at 1.23 V versus RHE, together with a combined $\eta_{abs} \times \eta_{sep}$ product of 53%. As far as we know, this is the great achievement to date in $BiVO_4$-based photoanodes (compared with the highest 45% previously reported). Furthermore, WO_3/W:$BiVO_4$ NWs were fabricated based on economical precursors via an low-cost and accurate process, which could significantly improve the efficiency of photoanodes for tandem PEC water-splitting systems.

$FE_{1-X}O$

Iron oxide is another important material for solar water splitting and is cheaper and widely distributed in the earth. Iron oxide has various forms, including FeO, Fe_3O_4 (magnetite), and Fe_2O_3 (hematite), with hematite (α-Fe_2O_3) exhibiting the desired properties.[84–86] α-Fe_2O_3 is a typical *n*-type semiconductor with the narrow bandgap (approximately 2.2 V), which possess large-scale absorption spectrum. The theoretical solar-to-hydrogen conversion efficiency (STH) of α-Fe_2O_3 is as high as 16.8%.[87] α-Fe_2O_3 NWs are normally synthesized based on the following three methods: atmospheric pressure, low pressure plasma, and thermal oxidation. Low-pressure plasma oxidation with continuous exposure over a few minutes can produce highly oriented, uniform, and dense NW arrays (Fig. 6a). The diameter of these NWs are ~100–300 nm at the base and tapered down to ~10 nm at the tips, and up to 5–10 μm in length. Figure 6b shows α-Fe_2O_3 NW arrays oxidized in a thermal furnace with high density, on the order of 5 μm in length, and tapered from 100 nm to 10 nm.

Because of the excellent physical and chemical properties, α-Fe_2O_3 has shown critical potentials in photocatalytism, especially in PEC. Chernomordik et al.[88] used three-electrode J–V tests to comparatively investigate the PEC performance of thermal and plasma oxidation-grown, hematite NW arrays. As a result, low-pressure plasma-oxidized samples produced much higher photocurrents than the thermally oxidized ones. The photocurrent of the hematite NW array electrodes prepared by thermal oxidation and plasma (low pressure, ICP) oxidation as shown in Fig. 7. The prepared samples exhibited significant photocurrents past 0 V versus SCE. At 1.5 V versus RHE, the photocurrent of the low-pressure plasma-assistant sample was 0.38 mA cm^{-2}, while thermally fabricated samples displayed negligible photocurrent. This study shows that hematite NWs prepared by direct plasma oxidation of iron, exhibit outstanding photoactivity.

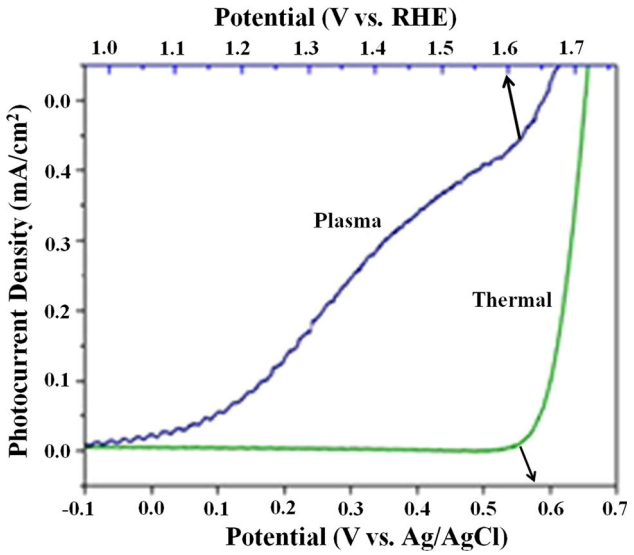

Fig. 7. Photoactivity of thermal oxidation and plasma oxidation grown hematite NW array electrodes. The plasma prepared sample exhibited a outstanding photocurrent of 0.38 mA cm^{-2} at 1.5 V versus RHE while thermally grown samples showed a negligible photoactivity. Reprinted from Ref. 88. Copyright 1990 CCC Republication.

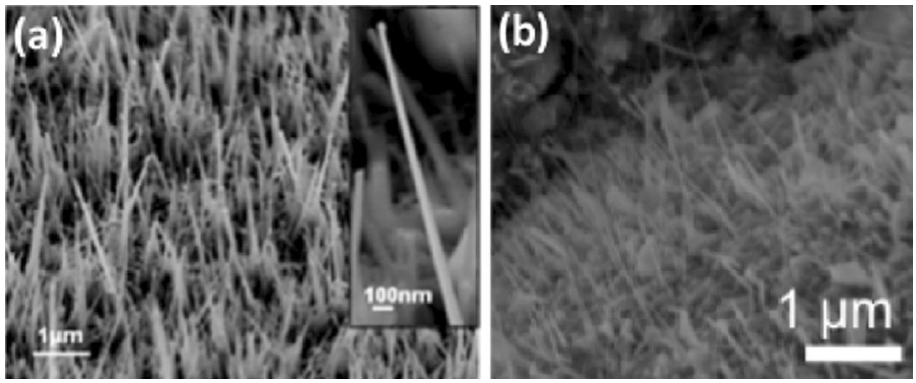

Fig. 6. SEM images of hematite NW arrays on iron substrates prepared under the following condition: (a) oxidation using low pressure (LP) ICP plasma; (b) oxidation in a thermal furnace. Reprinted from Ref. 88. Copyright 1990 CCC Republication.

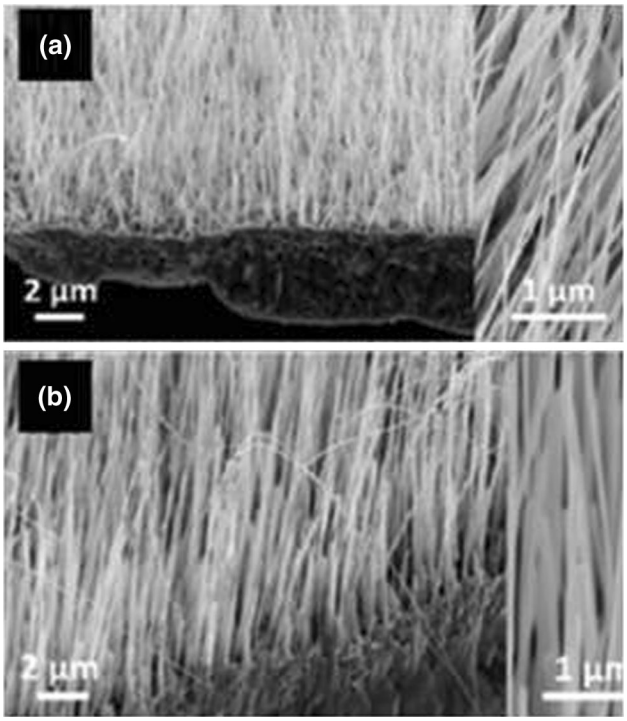

Fig. 8. SEM images of CuO NWs grown for 4 h on Cu foil at different annealing temperatures: (a) 400°C and (b) 500°C. The insets show the high-magnification images of the corresponding samples. Reprinted from Ref. 100. Copyright 2013 American Chemical Society.

CUO

CuO is another member of metal-oxide semiconductors that also possesses unique photocatalytic properties.[89–99] Copper oxides are extensively investigated in the application of water splitting. They are a naturally occurring *p*-type semiconductor and have suitable band gaps [$E_g \approx 1.4$ V (CuO), $E_g \approx 2.2$ V (Cu_2O)] for light absorption. Compared with bulk CuO, CuO NWs can enhance the PEC performance through its particular 1-D structures. Furthermore, stable materials such as TiO_2 coupled with the CuO in the heterostructure can enhance the efficiency of copper oxide photocathodes. Kargar et al.[100] demonstrated high efficiency 3-D ZnO/CuO branched NWs heterojunction photocathodes for PEC solar hydrogen production. Compared with core/shell NW heterostructures, the branched NWs (b-NWs) are very promising for PEC solar hydrogen production because of the large surface area.[101–103] CuO NW arrays can be synthesized on copper foil and mesh via thermal oxidation growth methods. Via simple, cost-effective thermal oxidation and hydrothermal growth methods, both pure CuO NW arrays and CuO/ZnO 5 m-ZnO/3 h-400°C-CuO (b-NWs) can be grown on different copper substrates with different NW sizes and densities. For example, Fig. 8a and b are the SEM images of CuO NW arrays grown in 400°C and 500°C, respectively, which demonstrates high temperature can produce longer, thicker, and denser CuO NW arrays than

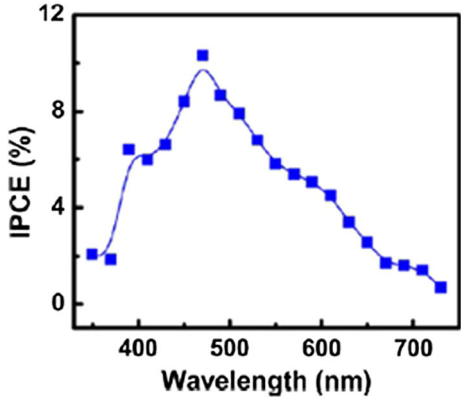

Fig. 9. Spectral IPCE of b-(5 m-ZnO/3 h-400°C-CuO) NWs at 0.4 V versus Ag/AgCl RE. Reprinted from Ref. 88. Copyright 2014 American Chemical Society.

low temperatures. Figure 9 further demonstrates the outstanding performance of ZnO/CuO b-NWs, over the spectral of IPCEs of b-NWs at −0.4 V. From 450 nm to 500 nm, the IPCEs are larger by 8% with a maximum efficiency of 10%. The ZnO/CuO b-NWs display broadband photoresponse from UV to the near IR region because of the coupling of narrow band gap CuO with wide band gap ZnO. This was produced by a facile and large-scale fabrication approach for 3-D ZnO/CuO b-NW photocathodes for solar hydrogen production in a neutral electrolyte. These results not only provide useful insights into the design and preparation of unique 3D b-NWs, but also exhibit critical potential in solar hydrogen production. Compared with CuO NWs, the ZnO/CuO b-NWs obviously display a significant advantage in photocatalysis. Although the stability of the CuO has been enhanced in this research, more in-depth work should be carried out to enhance the stability of *p*-type metal-oxides just like CuO. To our delight, b-NWs give us methods to enhance the photocatalytic properties of photocathodes by improve the structures of NWs.

CONCLUSIONS

Solar water splitting is one of the most promising approaches to relieve the energy shortage. Because of the unique chemical and physical properties, 1-D nanostructured metal oxides have been widely applied in solar water splitting. Among the vast majority of studied materials until now, semiconductor metal oxides such as Fe_2O_3, TiO_2, WO_3, ZnO, CuO have shown the most promising potential, partly because they are abundant, cheap, nontoxic, and can be fabricated via simple, low-cost, and scalable synthesis techniques (hydro/solvothermal growth method and electrodeposition). Although great progress has been made in the synthesis and application of highly efficient metal oxide NWs, several issues still remain unsolved. The short diffusion length, low conductivity, wide band gap, and poor surface evolution

kinetics of the metal oxides give raise to STH efficiencies considerably lower than their predicated theoretical values. Moreover, it is difficult to overcome the structure defects found in 1-D metal oxides. Extensive research is needed to design high quality metal oxide NWs for the application of solar water splitting. It is encouraging to see that many scientists have overcome challenges by optimizing one dimensional nanostructures, surface decoration, and doping. Hopefully, more and more useful research about 1-D metal oxides will be forthcoming.

ACKNOWLEDGEMENTS

This work was financially supported by the National Natural Science Foundation of China (Grant Number: 51402160), Natural Science Foundation of Shandong Province, China (Grant Number: ZR2014EMQ011), and the Applied Basic Research Foundation of Qingdao City (Grant Number: 14-2-4-45-jch), Taishan Scholar Program of Shandong Province, China.

REFERENCES

1. Y. Tachibana, L. Vayssieres, and J. Durrant, *Nat. Photonics* 6, 511 (2012).
2. N. Lewis and D. Nocera, *Proc. Natl. Acad. Sci.* 103, 15729 (2006).
3. M. Kanan and D. Nocera, *Science* 321, 1072 (2008).
4. M. Kröger, S. Hamwi, J. Meyer, T. Riedl, W. Kowalsky, and A. Kahn, *Org. Electron.* 10, 932 (2009).
5. S. Boettcher, E. Warren, M. Putnam, E. Santori, D. Turner-Evans, M. Kelzenberg, M. Walter, J.R. McKone, B. Brunschwig, and H. Atwater, *J. Am. Chem. Soc.* 133, 1216 (2011).
6. X. Michalet, F. Pinaud, L. Bentolila, J. Tsay, S. Doose, J. Li, G. Sundaresan, A. Wu, S. Gambhir, and S. Weiss, *Science* 307, 538 (2005).
7. G. Wang, Y. Ling, H. Wang, L.X. Hong, and Y. Li, *J. Photochem. Photobiol., B* 19, 35 (2014).
8. A. Fujishima, K. Honda, and B. Chem, *Soc. Jpn.* 44, 1148 (1971).
9. J. Lee, M. Orilall, S. Warren, M. Kamperman, F. DiSalvo, and U. Wiesner, *Nat. Mater.* 7, 222 (2008).
10. H. Bolink, E. Coronado, J. Orozco, and M. Sessolo, *Adv. Mater.* 21, 79 (2009).
11. A. Emeline, G. Kataeva, A. Panasuk, V. Ryabchuk, N. Sheremetyeva, and N. Serpone, *J. Phys. Chem.* 109, 5175 (2005).
12. G. Rignanese, *J. Phys.: Condens. Matter* 17, 357 (2005).
13. K. Chen, A. Bell, and E. Iglesia, *J. Catal.* 209, 35 (2002).
14. G. Mavrou, S. Galata, P. Tsipas, A. Sotiropoulos, Y. Panayiotatos, A. Dimoulas, E. Evangelou, J. Seo, and C. Dieker, *J. Appl. Phys.* 103, 4506 (2008).
15. R. Devan, R. Patil, J. Lin, and Y. Ma, *Adv. Funct. Mater.* 22, 3326 (2012).
16. A. Kudo and Y. Miseki, *Chem. Soc. Rev.* 38, 253 (2009).
17. X. Chen, S. Shen, L. Guo, and S. Mao, *Chem. Rev.* 110, 6503 (2010).
18. M. Walter, E. Warren, J. McKone, S. Boettcher, Q. Mi, E. Santori, and N. Lewis, *Chem. Rev.* 110, 6446 (2010).
19. D. Bavykin, V. Parmon, A. Lapkin, and F. Walsh, *J. Mater. Chem. A* 14, 3370 (2004).
20. G. Mor, K. Shankar, M. Paulose, O. Varghese, and C. Grimes, *Nano Lett.* 6, 215 (2006).
21. G. Mor, O. Varghese, M. Paulose, K. Shankar, and C. Grimes, *Sol. Energy Mater. Sol. Cells* 90, 2011 (2006).
22. G. Chen, C. Lee, H. Niu, W. Huang, R. Jann, and T. Schütte, *Thin Solid Films* 516, 8473 (2008).
23. M. Afifi, M. Abdel-Aziz, I. Yahia, M. Fadel, and L. Wahab, *J. Alloy. Compd.* 455, 92 (2008).
24. A. Kolmakov, Y. Zhang, G. Cheng, and M. Moskovits, *Adv. Mater.* 15, 997 (2003).
25. H. Senoh, Z. Siroma, N. Fujiwara, and K. Yasuda, *J. Power Sources* 185, 1 (2008).
26. S. Shi, Y. Zou, X. Cui, J. Xu, Y. Wang, G. Wang, G. Yang, J. Xu, T. Wang, and Z. Gao, *CrystEngComm* 12, 2122 (2010).
27. J. Piekoszewski, A. Krajewski, F. Prokert, J. Senkara, J. Stanisławski, L. Waliś, Z. Werner, and W. Włosiński, *Vacuum* 70, 307 (2003).
28. A. Wolcott, W. Smith, T. Kuykendall, Y. Zhao, and J. Zhang, *Small* 5, 104 (2009).
29. M. Paulose, K. Shankar, S. Yoriya, H. Prakasam, O. Varghese, G. Mor, T. Latempa, A. Fitzgerald, and C. Grimes, *J. Phys. Chem. B* 110, 16179 (2006).
30. A. Wolcott, W. Smith, T. Kuykendall, Y. Zhao, and J. Zhang, *Adv. Funct. Mater.* 19, 1849 (2009).
31. M. Seo, M. Yuasa, T. Kida, J. Huh, K. Shimanoe, and N. Yamazoe, *Sens. Actuators B Chem.* 137, 513 (2009).
32. A. Ghicov, H. Tsuchiya, R. Hahn, J. Macak, A. Muñoz, and P. Schmuki, *Electrochem. Commun.* 8, 528 (2006).
33. S. Berger, A. Ghicov, Y. Nah, and P. Schmuki, *Langmuir* 25, 4841 (2009).
34. G. Wang, H. Wang, Y. Ling, Y. Tang, X. Yang, R. Fitzmorris, C. Wang, J. Zhang, and Y. Li, *Nano Lett.* 11, 3026 (2011).
35. H. Kim and S. Kang, *Bull. Korean Chem. Soc.* 34, 2067 (2013).
36. S.Y. Noh, K. Sun, C. Choi, M. Niu, M. Yang, K. Xu, S. Jin, and D. Wang, *Nano Energy* 2, 351 (2013).
37. Y. Lin, G. Yuan, R. Liu, S. Zhou, S. Sheehan, and D. Wang, *Chem. Phys. Lett.* 507, 209 (2011).
38. A. Fujishima, *Nature* 238, 37 (1972).
39. R. Rocheleau and E. Miller, *Int. J. Hydrogen Energy* 22, 771 (1997).
40. Y. Pu, G. Wang, K. Chang, Y. Ling, Y. Lin, B. Fitzmorris, C. Liu, X. Lu, Y. Tong, and J. Zhang, *Nano Lett.* 13, 3817 (2013).
41. Z. Liu, W. Hou, P. Pavaskar, M. Aykol, and S. Cronin, *Nano Lett.* 11, 1111 (2011).
42. Y. Wang, Q. Wang, X. Zhan, F. Wang, M. Safdar, and J. He, *Nanoscale* 5, 8326 (2013).
43. T. Kong, Y. Chen, Y. Ye, K. Zhang, Z. Wang, and X. Wang, *Sens. Actuators B Chem.* 138, 344 (2009).
44. A. Qurashi, N. Tabet, M. Faiz, and T. Yamzaki, *Nanoscale Res. Lett.* 4, 948 (2009).
45. Y. Masuda, T. Ohji, and K. Kato, Tin oxide nanosheet assembly for hydrophobic/hydrophilic coating and cancer sensing. *ACS Appl. Mater. Interfaces.* 4, 1666 (2012).
46. O. Lupan, T. Pauporté, T. Le Bahers, B. Viana, and I. Ciofini, *Adv. Funct. Mater.* 21, 3564 (2011).
47. W. Wang, B. Zeng, J. Yang, B. Poudel, J. Huang, M. Naughton, and Z. Ren, *Adv. Mater.* 18, 3275 (2006).
48. H. Zeng, X. Xu, Y. Bando, U. Gautam, T. Zhai, X. Fang, B. Liu, and D. Golberg, *Adv. Funct. Mater.* 19, 3165 (2009).
49. L. Vayssieres, *Adv. Mater.* 15, 464 (2003).
50. M. Huang, S. Mao, H. Feick, H. Yan, Y. Wu, H. Kind, E. Weber, R. Russo, and P. Yang, *Science* 292, 1897 (2001).
51. G. Shen, Y. Bando, B. Liu, D. Golberg, and C. Lee, *Adv. Funct. Mater.* 16, 410 (2006).
52. U. Gautam, L. Panchakarla, B. Dierre, X. Fang, Y. Bando, T. Sekiguchi, A. Govindaraj, D. Golberg, and C. Rao, *Adv. Funct. Mater.* 19, 131 (2009).
53. A. Wei, X.W. Sun, C. Xu, Z. Dong, M. Yu, and W. Huang, *Appl. Phys. Lett.* 88, 213102 (2006).
54. Y. Tseng, C. Huang, H. Cheng, I. Lin, K. Liu, and I. Chen, *Adv. Funct. Mater.* 13, 811 (2003).
55. U. Manzoor and D. Kim, *Scripta Mater.* 54, 807 (2006).
56. Y. Leung, A. Djurišić, J. Gao, M. Xie, Z. Wei, S. Xu, and W. Chan, *Chem. Phys. Lett.* 394, 452 (2004).
57. C. Lao, P. Gao, R. Yang, Y. Zhang, Y. Dai, and Z. Wang, *Chem. Phys. Lett.* 417, 358 (2006).
58. C. Xu and X. Sun, *Appl. Phys. Lett.* 83, 3806 (2003).

59. Y. Zhu, H. Zhang, X. Sun, S. Feng, J. Xu, Q. Zhao, B. Xiang, R. Wang, and D. Yu, *Appl. Phys. Lett.* 83, 144 (2003).
60. Y. Xu, H. Rao, X. Wang, H. Chen, D. Kuang, and C. Su, *J. Mater. Chem. A* 4, 5124 (2016).
61. X. Wang, Y. Ding, C. And, and L. Zhong, *J. Phys. Chem. B* 108, 8773 (2004).
62. S. Minne, S. Manalis, and C. Quate, *Appl. Phys. Lett.* 67, 3918 (1995).
63. L. Guo, Y. Ji, H. Xu, P. Simon, and Z. Wu, *J. Am. Chem. Soc.* 124, 14864 (2002).
64. C. Liu, J. Zapien, Y. Yao, X. Meng, C. Lee, S. Fan, Y. Lifshitz, and S. Lee, *Adv. Mater.* 15, 838 (2003).
65. L. Vayssieres, K. Keis, A. Anders Hagfeldt, and S. Lindquist, *Chem. Mater.* 13, 4395 (2001).
66. S. Nandi, S. Chakraborty, M. Bera, and C. Maiti, *Bull. Mater. Sci.* 30, 247 (2007).
67. Y. Ding, X. Kong, and Z. Wang, *Phys. Rev. B* 70, 235408 (2004).
68. Y. Koh, M. Lin, C. Tan, Y. Foo, and K. Loh, *J. Phys. Chem. B* 108, 11419 (2004).
69. H. Lee, S. Shin, K. Nam, J. Nah, and M. Lee, *J. Mater. Chem. A* 4, 3223 (2016).
70. Y. Ma, C. Lin, C. Yeh, and R. Huang, *J. Vac. Sci. Technol., B* 23, 2141 (2005).
71. P. Woodward, A. Sleight, and T. Vogt, *J. Solid State Chem.* 131, 9 (1997).
72. W. Hu, Y. Zhu, W. Hsu, B. Chang, M. Terrones, N. Grobert, H. Terrones, J. Hare, H. Kroto, and D. Walton, *Appl. Phys. A* 70, 231 (2000).
73. H. Choi, Y. Jung, and D. Kim, *J. Am. Ceram. Soc.* 88, 1684 (2005).
74. R. Hu, H. Wu, and K. Hong, *J. Cryst. Growth* 306, 395 (2007).
75. M. Zumer, V. Nemanič, B. Zajec, M. Wang, J. Wang, Y. Liu, and L. Peng, *J. Phys. Chem. C* 112, 5250 (2008).
76. Y. Zhao, Y. Li, I. Ahmad, D. McCartney, Y. Zhu, and W. Hu, *Appl. Phys. Lett.* 89, 133116 (2006).
77. T. Zhai, L. Li, X. Wang, X. Fang, Y. Bando, and D. Golberg, *Adv. Funct. Mater.* 20, 4233 (2010).
78. K. Liu, D.T. Foord, and L. Scipioni, *Nanotechnology* 16, 10 (2004).
79. G. Gu, B. Zheng, W. Han, S. Roth, and J. Liu, *Nano Lett.* 2, 849 (2002).
80. C. Chen, S. Wang, R. Ko, Y. Kuo, K. Uang, T. Chen, B. Liou, and H. Tsai, *Nanotechnology* 17, 217 (2005).
81. J. Liu, Y. Zhao, and Z. Zhang, *J. Phys.: Condens. Matter* 15, L453 (2003).
82. J. Zhou, L. Gong, S. Deng, J. Chen, J. She, N. Xu, R. Yang, and Z. Wang, *Appl. Phys. Lett.* 87, 223108 (2005).
83. P. Rao, L. Cai, C. Liu, I. Cho, C. Lee, J. Weisse, P. Yang, and X. Zheng, *Nano Lett.* 14, 1099 (2014).
84. Y. Hu, A. Kleiman-Shwarsctein, A. Forman, D. Hazen, J. Park, and E. McFarland, *Chem. Mater.* 20, 3803 (2008).
85. I. Cesar, A. Kay, J.A. Gonzalez Martinez, and M. Grätzel, *J. Am. Chem. Soc.* 128, 4582 (2006).
86. J. Turner, M. Hendewerk, J. Parmeter, D. Neiman, and G. Somorjai, *J. Electrochem. Soc.* 131, 1777 (1984).
87. A. Murphy, P. Barnes, L. Randeniya, I. Plumb, I. Grey, M. Horne, and J. Glasscock, *Int. J. Hydrogen Energy* 31, 1999 (2006).
88. B. Chernomordik, H. Russell, U. Cvelbar, J. Jasinski, V. Kumar, T. Deutsch, and M. Sunkara, *Nanotechnology* 23, 194009 (2012).
89. Y. Qiu, K. Yan, H. Deng, and S. Yang, *Nano Lett.* 12, 407 (2012).
90. A. Paracchino, N. Mathews, T. Hisatomi, M. Stefik, S. Tilley, and M. Grätzel, *Energy Environ. Sci.* 5, 8673 (2012).
91. S. Warren and E. Thimsen, *Energy Environ. Sci.* 5, 5133 (2012).
92. A. Paracchino, V. Laporte, K. Sivula, M. Grätzel, and E. Thimsen, *Nat. Mater.* 10, 456 (2011).
93. J. Su, X. Feng, J. Sloppy, L. Guo, and C. Grimes, *Nano Lett.* 11, 203 (2011).
94. G. Wang, Y. Ling, H. Wang, X. Yang, C. Wang, J. Zhang, and Y. Li, *Energy Environ. Sci.* 5, 6180 (2012).
95. X. Zhao, P. Wang, and B. Li, *Chem. Commun.* 46, 6768 (2010).
96. W.M. Jin, J. Kang, and J. Moon, *ACS Appl. Mater. Interfaces.* 2, 2982 (2010).
97. Z. Zhang and P. Wang, *J. Mater. Chem.* 22, 2456 (2012).
98. A. Kargar, S. Partokia, M. Niu, P. Allameh, M. Yang, S. May, J. Cheung, K. Sun, K. Xu, and D. Wang, *Nanotechnology* 25, 696 (2014).
99. W. Siripala, A. Ivanovskaya, T. Jaramillo, S. Baeck, and E. Mcfarland, *Sol. Energy Mater. Sol. C* 77, 229 (2003).
100. A. Kargar, Y. Jing, S. Kim, C. Riley, X. Pan, and D. Wang, *ACS Nano* 7, 11112 (2013).
101. C. Cheng and H. Fan, *Nano Today* 7, 327 (2012).
102. A. Kargar, K. Sun, Y. Jing, C. Choi, H. Jeong, G.Y. Jung, S. Jin, and D. Wang, *ACS Nano* 7, 9407 (2013).
103. A. Kargar, K. Sun, Y. Jing, C. Choi, H. Jeong, Y. Zhou, K. Madsen, P. Naughton, S. Jin, and G. Jung, *Nano Lett.* 13, 3017 (2013).